Mesoscale Elucidation of Solid Electrolyte Interphase Layer Formation in Li-ion Battery Anode

Feng Hao,[1] Zhixiao Liu,[2] Perla B. Balbuena,[3] and Partha Mukherjee[1,*]

[1]School of Mechanical Engineering, Purdue University, West Lafayette, IN 47907, USA
[2]College of Materials Science and Engineering, Hunan University, Changsha 410082, China
[3]Department of Chemical Engineering, Texas A&M University, College Station, TX 77843, USA

Manuscript submitted to

The Journal of Physical Chemistry C

September 2017

[*]*Correspondence*: pmukherjee@purdue.edu

Abstract

Capacity fade in lithium-ion batteries largely originates from the undesired electrolyte decomposition, which results in the formation of solid electrolyte interphase (SEI) and the anode surface passivation. In this work, a mesoscale interfacial modeling approach is developed for investigating the formation and growth of the SEI film on typical graphite based anode over several cycles. It is found that Li diffusion kinetics in the SEI film significantly affects the SEI growth rate. Lower Li diffusion barrier leads to higher growth rate. The present model demonstrates that the SEI thickness is a linear function of the square root of the charging time over long-time cycling. Growth of multi-component SEI film is also elucidated. It is found that the heterogeneity of the SEI film may lead to instability in Li ion concentration distribution.

1. Introduction

Li-ion batteries have attracted intense research interest, in particular, because of the emerging demand for electric vehicles. Prominent advantages include high specific capacities and operating voltages, resulting in the widespread use of lithium-ion batteries as energy storage devices [1,2]. During the charging/discharging operation, a solid electrolyte interphase (SEI) layer gradually forms on the graphite surface, generated by the decomposition products of the solvent and lithium salt [3,4], beginning around 0.8 V vs. Li/Li^+ [5]. The SEI formation determines the initial capacity loss and long-term capacity retention, given that its growth continuously consumes Li. The electronically insulating SEI film is expected to possess high Li ion permeability to enhance the Li transport kinetics and alleviate the anode surface passivation. Therefore, the SEI stability is of great significance to the cycling performance, which can be improved by solvent additives and surface modifications of the electrode [6,7].

In general, the SEI is composed of densely packed inorganic compounds and loosely aggregated organic components on the electrolyte side, and its chemical composition depends on the solvents, electrolyte salts, and electrode materials used in Li-ion batteries. The common inorganic compounds include Li_2CO_3, LiF, and Li_2O, which are non-uniformly distributed in the SEI layer [8,9]. Owing to its complexity, the SEI formation mechanism is a major topic of debate, including topics such as the reduction pathways of solvent and salt anion molecules [10]. Despite the assumed high electronic resistance, the SEI layer grows during repeated charging-discharging cycles, stemming from electron tunneling to the electrolyte phase or electrolyte transfer to the anode surface.

The ultra-thin SEI, few nanometers to tens of nanometers, is sensitive to ambient conditions, rendering experimental measurements difficult. In addition to experiments [11,12], theoretical and computational studies are used to understand the intricate reactions and SEI growth on the electrode surface based on molecular dynamics (MD), first-principles simulations [13-16], kinetic Monte Carlo (KMC) method [17], and macroscopic modeling approaches [18,19]. For example, Röder *et al*. recently reported a multi-scale simulation strategy to investigate the SEI growth, which couples a macroscopic model with the KMC algorithm [20].

As for the theoretical models, it is impossible to capture all the reactions in practical Li-ion batteries. Here, the scope of our study is restricted to the model shown in Fig. 1. The overall negative electrode reaction is composed of a series of steps during the charging process, including the adsorption of reactants (Li-ion and solvent) to the SEI upper surface, the diffusion of reactants through the SEI film, and the electrochemical reactions at the electrode-SEI interface. It should be mentioned that SEI is considered as an insulator for electron flow in Fig. 1, and new SEI forms due to the reduction of solvents. Following the previous studies [21,22], solvents need to diffuse through the already existed SEI layer to the electrode-SEI interface and then reacts with Li-ion and electrons.

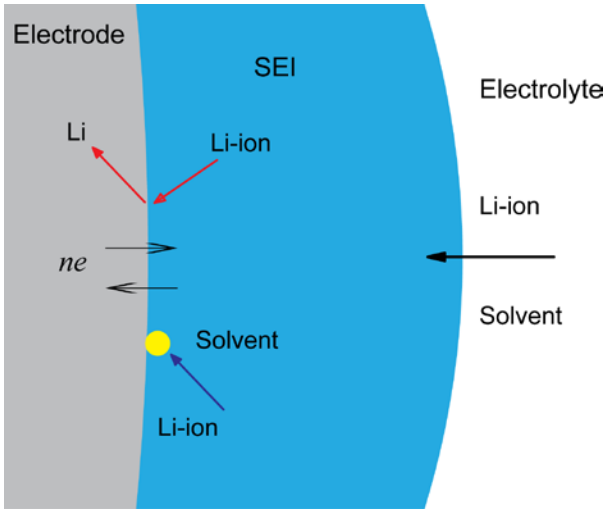

Fig. 1. Schematic of the redox reactions at the electrode-electrolyte interface, including Li intercalation into the electrode after reduced and new SEI formation caused by the reaction of Li-ion with solvent.

Li-ion diffusion in the SEI film plays a pivotal role in the subsequent reactions, including Li reduction and intercalation into active materials, as well as the SEI formation on the electrode surface. Therefore, a coupled KMC model is developed to relate the Li-ion diffusion kinetics to the SEI growth, which is not addressed in previous KMC models [17,20]. In addition, Li-ion diffusion in the two-phase SEI film is explored, and the Li content distribution in SEI is found to be greatly affected by the nature of the heterogeneous SEI. This work provides a fundamental understanding of SEI formation and growth during the charging operation in Li-ion batteries, shedding light on the effect of Li-ion transport kinetics on SEI growth.

2. Model and Method

Fig. 1 depicts the three steps in the KMC model. First, it involves Li-ion adsorption and solvent adsorption on the SEI film surface near the electrolyte. Then, Li-ion and solvent diffuse through the SEI layer and reach the electrode-SEI interface [21]. Following the electron transfer, Li-ion is reduced and then intercalates into the electrode; otherwise, Li-ion reacts with the solvent to produce new SEI. In this work, the net current is mainly governed by the inherent sluggishness of the latter two steps. The electron transfer, Li intercalation into the electrode, and the mass transfer of reactants in the electrolyte are assumed to be fast enough and thus not involved in our KMC model. The rates for the three steps are introduced in the following.

At the electrode-SEI interface, two redox systems are considered in our model. The first is $Li^+ + e \leftrightarrow Li$, and the reduced Li intercalates into active materials. The faradaic current generated by the reaction is estimated by using the Butler-Volmer equation

$$J_0 = i_0\left(\exp\left(-\frac{\alpha F}{RT}\eta\right) - \exp\left(\frac{\beta F}{RT}\eta\right)\right). \tag{1}$$

The first term represents the Li reduction from SEI to the electrode, and the second term is for Li oxidation from the electrode to SEI. In practice, the latter is much smaller than the former during battery charging. R is the gas constant, T is the operating temperature, and F is the Faraday constant. α and β are charge transfer coefficients which yield $\alpha + \beta = 1$. i_0 is the exchange current density of Li reduction at the anode-SEI interface, which is given as

$$i_0 = C_1 c_{Li^+}^{\alpha} c_{Li}^{\beta} = C_0 \frac{c_{Li^+}}{c_{M(Li^+)}}. \tag{2}$$

Here C_1 is a constant, α and β are charge transfer coefficients, and c_{Li^+} and $c_{M(Li^+)}$ are the actual Li-ion concentration and Li-ion concentration limit at the anode-SEI interface, which is related to the site occupation ratio of Li-ion in the lattice of the active electrode surface or SEI bottom layer in the simulation. Here, Eq. (2) implies that the reduced Li concentration at the interface c_{Li} is assumed to be linearly dependent on c_{Li^+}. C_0 is the exchange current density at $c_{Li^+} = c_{M(Li^+)}$, which holds when the overall current is controlled by the Li-ion reduction rates on the electrode surface. For Li-ion batteries, the exchange current density of graphite is 1-2.3 mA/cm^2 [23], much larger than that of silicon (0.1 mA/cm^2) [24]. η is the overpotential driving the electrochemical reactions, which is defined as

$$\eta = \phi_{electrode} - \phi_{electrolyte} - U + JR_{SEI}, \tag{3}$$

$$J = J_0 + J_{SEI}. \tag{4}$$

where $\phi_{electrode}$, $\phi_{electrolyte}$, and U are the negative electrode potential, electrolyte potential, and equilibrium negative electrode potential, respectively. J is the total current density, consisting of J_0 and J_{SEI} addressed below, and R_{SEI} is the resistance of the SEI layer. Thus, the last term in Eq. (3) stands for the potential change stemming from the SEI growth.

The second redox system considered is the reaction of $2Li^+ + E + 2e \leftrightarrow Li_2E$, where E is the solvent from the electrolyte, and Li_2E is the product leading to the SEI formation. Herein, we assume that the reactant and product engage in a two-electron transfer. A one-electron reduction can be implemented by extending the current model. The current density is described by the Butler-Volmer kinetics

$$J_{SEI} = i_{SEI}\left(\exp\left(-\frac{\alpha_{SEI}F}{RT}\eta_{SEI}\right) - \exp\left(\frac{\beta_{SEI}F}{RT}\eta_{SEI}\right)\right), \tag{5}$$

where α_{SEI} and β_{SEI} are transfer coefficients and both set to be 0.5, see in Table 1. Similar to Eq. (2), the exchange current density i_{SEI} for SEI growth is written as

$$i_{SEI} = C_{SEI}\frac{c_{S-Li^+}}{c_{M(S-Li^+)}}, \tag{6}$$

c_{S-Li^+} is the concentration of the mixture of solvent and Li-ion at the electrode-SEI interface, and it requires that solvent and Li-ion co-exist at one lattice site of the active electrode surface; meanwhile, at least one of its adjacent site is occupied by Li-ion. $c_{M(S-Li^+)}$ is the concentration limit of c_{S-Li^+}. C_{SEI} is the maximum exchange current density of i_{SEI} at $c_{S-Li^+} = c_{M(S-Li^+)}$. The current density J_{SEI} is driven by the overpotential η_{SEI}

$$\begin{aligned}\eta_{SEI} &= \phi_{electrode} - \phi_{electrolyte} - U_{SEI} + JR_{SEI} \\ &= (\eta + U) - U_{SEI} \\ &= \phi - U_{SEI}\end{aligned} \tag{7}$$

U_{SEI} is the equilibrium potential for SEI formation, around 0.8 V [25]. In this work, the sum of η and U is assumed as

$$\begin{aligned}\phi = {} & 0.7122 + 0.1387\gamma + 0.029\gamma^{0.5} - 0.0172\gamma^{-1} + 0.0019\gamma^{-1.5} \\ & + 0.2808\exp(0.9 - 15\gamma) - 0.7984\exp(0.4465\gamma - 0.4108),\end{aligned} \tag{8}$$

where γ is the charge depth or state of charge, obtained by the ratio of the number of Li intercalated into the electrode to the number of Li up to the capacity limit of an electrode [17].

For a single lattice site in the KMC model, the rates of the above two redox systems are thus deduced by using Eqs. (1) and (5)

$$k_0 = \frac{J_0 a^2}{F} N_a, \tag{9}$$

$$k_{SEI} = \frac{J_{SEI} a^2}{F} N_a. \tag{10}$$

Where a is the size of one lattice cell, and N_a is the Avogadro constant.

Supposing that Li diffusion and solvent diffusion in the SEI film obey the hopping mechanism, the rate is thus described by Arrhenius formulation

$$k = \nu \exp\left(\frac{-E_a}{RT}\right), \tag{11}$$

ν is the jumping frequency for Li^+ (or solvent) diffusion, approximately 10^{12}~10^{13} s^{-1}. E_a is the activation energy for the species diffusion in the SEI, i.e. the height of the barrier needed to be overcome.

The setup of the above steps applies to electrodes of various shapes. In this work, the spherical electrode is taken as an example, and the radius is 300 nm if no other note is given. The charging is conducted under galvanostatic condition. In this circumstance, the overpotential of Li-ion reduction is fixed to be -0.1 V, which ensures that J_0 is almost constant during charging. The activation energies of the reactants are 38.4-76.8 KJ/mol, which are among the reported ones [26,27]. At the electrode-SEI interface, the lattice is a 30×30 grid of 900 sites in the KMC model. The simulation runs until the electrode is fully charged at γ = 100%. All the parameters used are listed in Table 1.

Table 1. Parameters used in the KMC model.

Parameters		Values	Units
C_0	Exchange current density for Li	1	mA/cm^2

	reduction		
C_{SEI}	Exchange current density for SEI growth	0.1	mA/cm^2
η	Overpotential for Li reduction	-0.1	V
U_{SEI}	Equilibrium potential for SEI growth	0.8	V
α, β, α_{SEI}, β_{SEI}	Charge transfer coefficients	0.5	
E_a	Activation energy for diffusion in SEI	38.4-76.8	KJ/mol
k_{Li}	Li adsorption rate	100,000	1/s
k_S	Solvent adsorption rate	1000	1/s
C_{max}	Maximum Li concentration in anode	3,1500	mol/m^3
R_p	Particle radius	300	nm
a	lattice cell dimension	0.5	nm
R	Gas constant	8.314	J/mol/K
F	Faraday constant	96,487	C/mol
N_a	Avogadro constant	6.022×10^{23}	1/mol
T	Operating temperature	200–320	K
v	Vibration frequency	5×10^{12}	1/s

3. Results and discussion

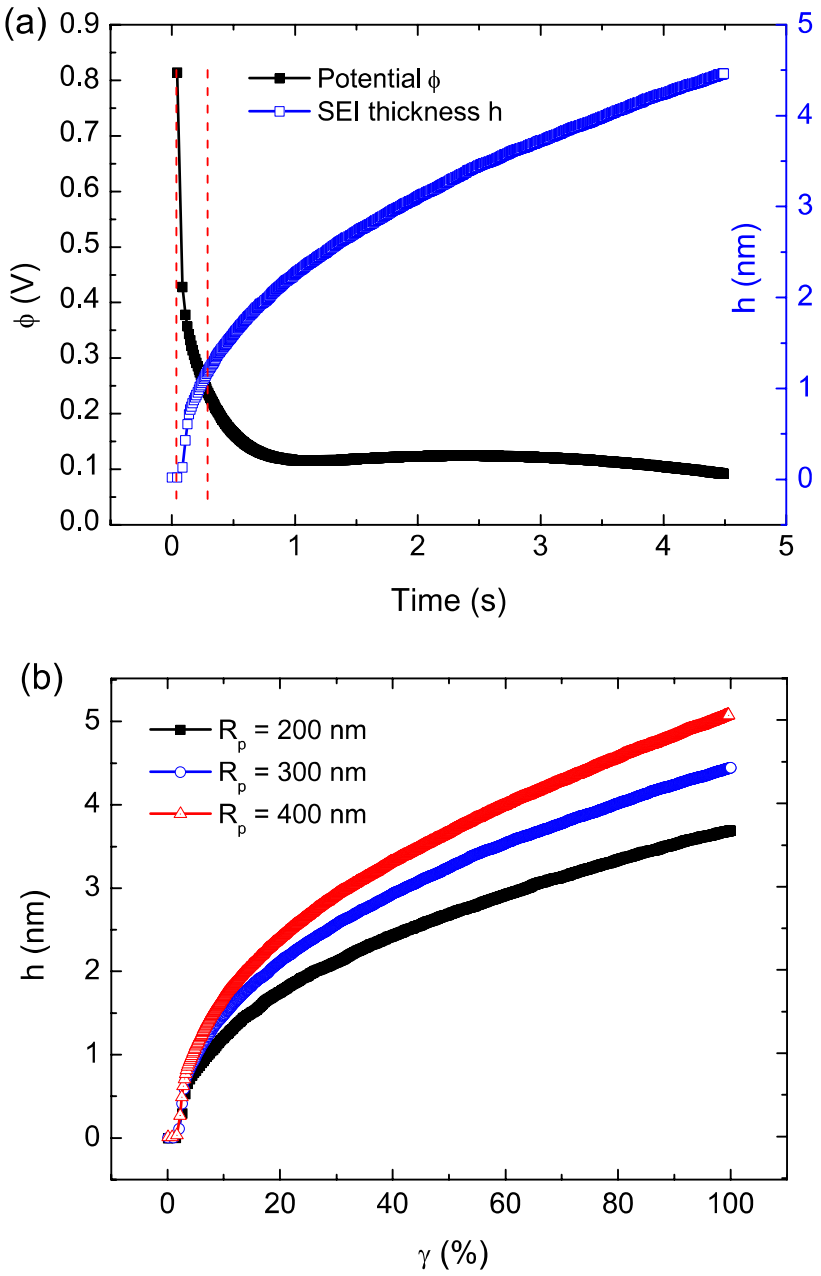

Fig. 2. (a) Potential ϕ and SEI growth on the anode surface with increasing time during the first charging, where R_p = 300 nm, E_a = 46.1 KJ/mol for Li-ion activation energy in SEI, and E_a = 67.2 KJ/mol for the activation energy of solvent diffusion in SEI. I, II, and III represent the three stages of SEI growth. (b) SEI growth profiles for single particles with various radii.

Fig. 2(a) shows the potential ϕ and SEI growth on the negative electrode during the first charging cycle. The activation energy of Li-ion diffusion in SEI is 46.1 KJ/mol, and 67.2 KJ/mol for solvent diffusion. The total charging time is only 4.49 s for a spherical electrode with the radius of R_p = 300 nm, which is due to the relatively high overpotential and the steady current over the single particle surface in our model. In practical batteries, the negative electrode film is composed of a number of micro-particles in the film thickness direction, and the current density could not be uniform on the particle surfaces, and thus the charging time will be much longer. In fact, the total charging time can be estimated by the expression

$$t_M = \frac{FC_{\max}}{3J_0} R_p. \tag{12}$$

Considering that Li-ion reduction is the rate-determining step for the parameters set in Fig. 2, the exchange current density i_0 in Eq. (2) approximates to C_0. Therefore, Eq. (12) yields t_M = 4.47 s, which is close to 4.49 s in the simulation, and thus it confirms the accuracy of our KMC model. The slight discrepancy is caused by Li-loss for the SEI formation and calculation errors.

There are three distinct stages of the SEI growth during the first charge in Fig. 2: roughly I (ϕ > 0.8 V and h = 0), II (0.3 V < ϕ < 0.8 V and h < 1 nm), and III (ϕ < 0.3 V and h > 1 nm). Little SEI is formed at the initial charging stage, which is consistent with the reported results that the decomposition of solvent and SEI formation begins around 0.8 V *vs.* Li/Li^+ [5,25,28]. As the potential reduces to 0.8 V, a rapid SEI growth takes place at the second stage, because of the abundant solvent absorbed on the

negative electrode surface. As the charging proceeds, the initial accumulated solvent is fully consumed, and then the solvent has to diffuse through the SEI layer to the electrode surface to support the electrochemical reactions producing new SEI. As a result, the SEI growth rate is gradually lowered at the third stage. Fig. 2(b) shows the SEI growth curves for electrodes with different radii. It is evident that the larger the electrode size is, the thicker the SEI grows. According to the Eq. (12), the large particle takes a relatively long time to become fully charged, which enables more time for the SEI growth, and the dependence of the SEI thickness on the charging time will be addressed in a later section.

Fig. 3(a) provides Li-ion content profiles in the SEI film with varying time, where the parameters are the same as used in Fig. 2(a). The distance begins from the electrode-SEI interface (set as 0) to the upper SEI surface. The three curves are calculated at the charging times of 0.62 s, 2.07 s, and 4.48 s, showing the similar trend in the thickness direction. c_{CM} is the maximum content, corresponding to the configuration in which Li-ions occupy all the 900 sites in the same layer. Obviously, Li-ion concentration is very high at the electrode-SEI interface during the charging cycle. It implies that Li-ion reduction is much more sluggish than all the other steps so that it controls the rate of Li intercalation. A distinct feature is that the Li-ion content dramatically decreases at the end of each curve, originating from the surface roughness of SEI near the electrolyte (Li-ions in the electrolyte are not included in the profiles). Fig. 3(b) and (c) depict the SEI morphologies at times of 0.62 s and 2.07 s, respectively. For the rough surface, the SEI thickness refers to the average thickness in this work.

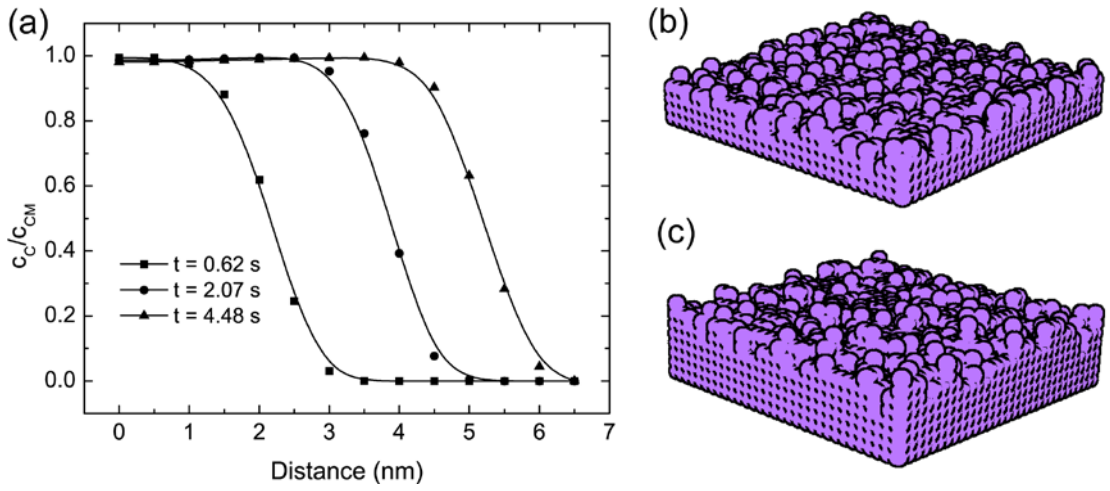

Fig. 3. (a) Li-ion content profiles in SEI with varying times during the first charging, where the activation energies are 46.1 KJ/mol and 67.2 KJ/mol for Li-ion and solvent, respectively. (b) and (c) are SEI morphologies at times of 0.62 s and 2.07 s, respectively.

Li-ion transport through the SEI layer plays a pivotal role in the negative electrode reactions, including Li reduction and intercalation into active materials, as well as the SEI formation. Therefore, the effect of Li-ion diffusion kinetics on the electrochemical behaviors is investigated. The activation energy of Li-ion diffusion in SEI ranges from 38.4 KJ/mol to 57.6 KJ/mol, and the solvent activation energy is fixed at 67.2 KJ/mol. In Fig. 4(a), it can be seen that there are no significant changes when the activation energy is below 46 KJ/mol. However, as the activation energy exceeds 46 KJ/mol, the total charging time and SEI thickness both increase for the first charging cycle.

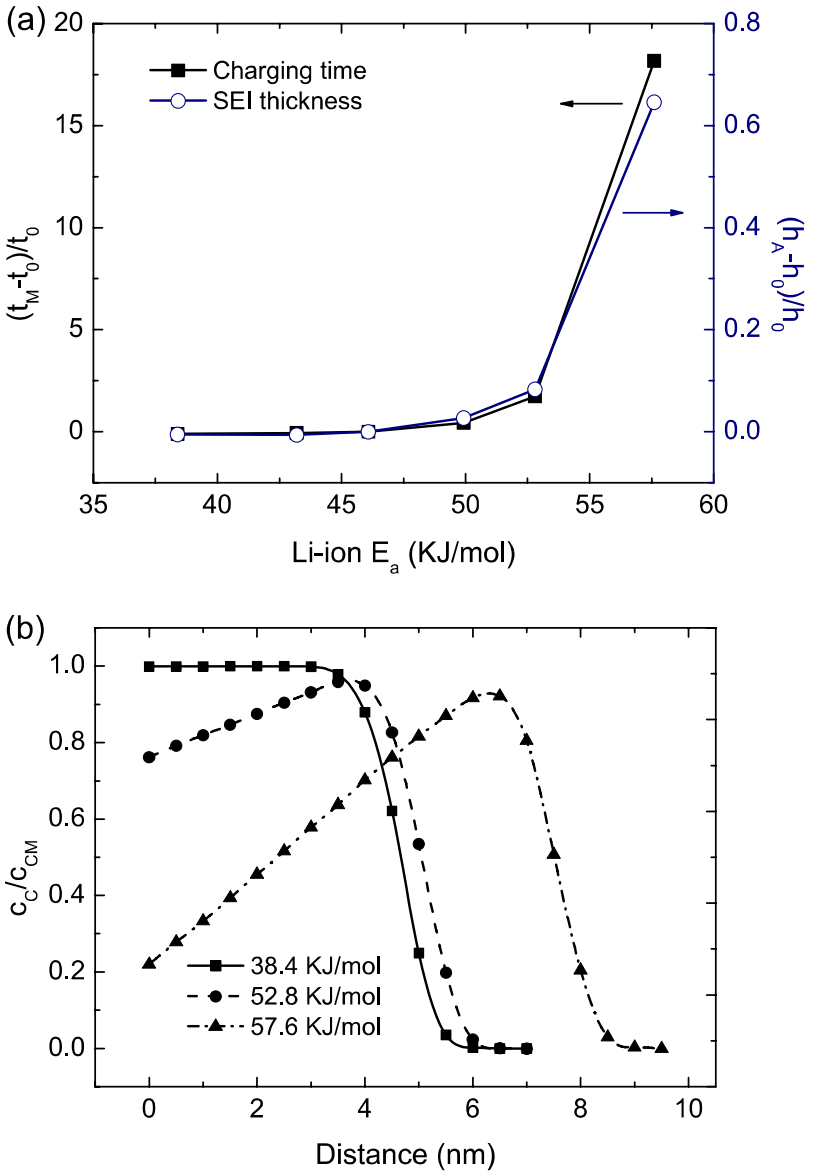

Fig. 4. (a) The effects of Li-ion activation energy in SEI on the total charging time and SEI thickness during a full charging process. (b) The influence of Li activation energy on the Li content profile in SEI.

Fig. 4(b) shows the Li-ion content in the thickness direction when the diffusion reaches the steady state. As the transport resistance increases, Li-ion content decreases at the electrode-SEI interface, which leads to the reduced current density shown in Eq. (1) and (2), thereby increasing the total charging time. In other words, Li-ion transfer

in the SEI layer becomes the rate-determining step for the overall electrode reactions, which increases the concentration overpotential in the battery because of the Li-ion content gradient through the SEI film. In this situation, the applied potential on the negative electrode should be lowered during charging, to ensure the charging rate. The results demonstrate that fast Li-ion transport kinetics is of great importance for Li-ion batteries. Therefore, a porous SEI, contributing to the fast Li-ion diffusion, is necessary to improve the electrochemical performance.

Li-ion transport kinetics affects the SEI growth by changing the total charging time, while the SEI growth rate is directly related to the solvent transport kinetics in SEI, which is illustrated in Fig. 5(a). The activation energy of solvent diffusion in the SEI ranges from 62.4 KJ/mol to 76.8 KJ/mol, and the solvent activation energy is fixed at 46.1 KJ/mol. According to Eq. (11), an increase of 5.53 KJ/mol in activation energy produces one order of magnitude decrease in the diffusion rate. Fig. 5(a) shows that as the solvent transport resistance increases, the SEI thickness is greatly shrunk. In addition, the total charging time is slightly reduced with increasing solvent activation energy in the SEI, which is attributed to the following competition. At the electrode-SEI interface, two reactions associated with Li consumption are considered, corresponding to the Li intercalation into the electrode and the formation of SEI. Because the content of solvent available at the interface decreases with increasing activation energy for solvent transport, Li-loss for the reaction with solvent is reduced. Thus, some Li atoms intercalate into the electrode instead of forming new SEI, which eventually shortens the total charging time. Fig. 5(b) depicts the SEI thickness contour,

which visualizes the effect of activation energy of reactant transfer in SEI on the passivation film thickness after the first charge. In practice, the SEI film should be thin enough to reduce the resistance and thick enough to completely protect the active materials, ensuring the high electrochemical performance of Li-ion batteries.

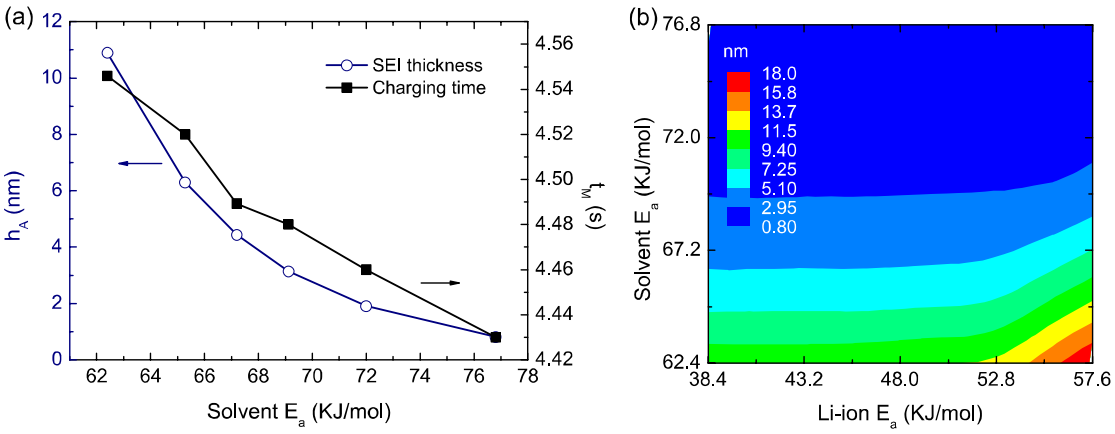

Fig. 5. (a) The effects of solvent activation energy in SEI on the total charging time and SEI thickness during a full charging process. (b) SEI thickness contour under various activation energies of Li-ion and solvent.

In Fig. 6, the temperature effect is investigated, considering that Li-ion batteries could experience low or elevated temperature operation. As the temperature rises, it accelerates the SEI growth, which is consist with the previous experiments and models [11,22]. Initially, Li intercalation rate is governed by the Li reduction rate in Eq. (1), thus the total charging time is shortened as the temperature drops due to the increased current density in Eq. (1). However, as the Li-ion transport resistance in the SEI

increases with decreasing temperature, Li-ion transport will become the rate-determining step for Li intercalation. Therefore, there exists a turning point in the curve of total charging time, approximately 250 K in Fig. 6, and the total charging time begins to increase below this critical temperature.

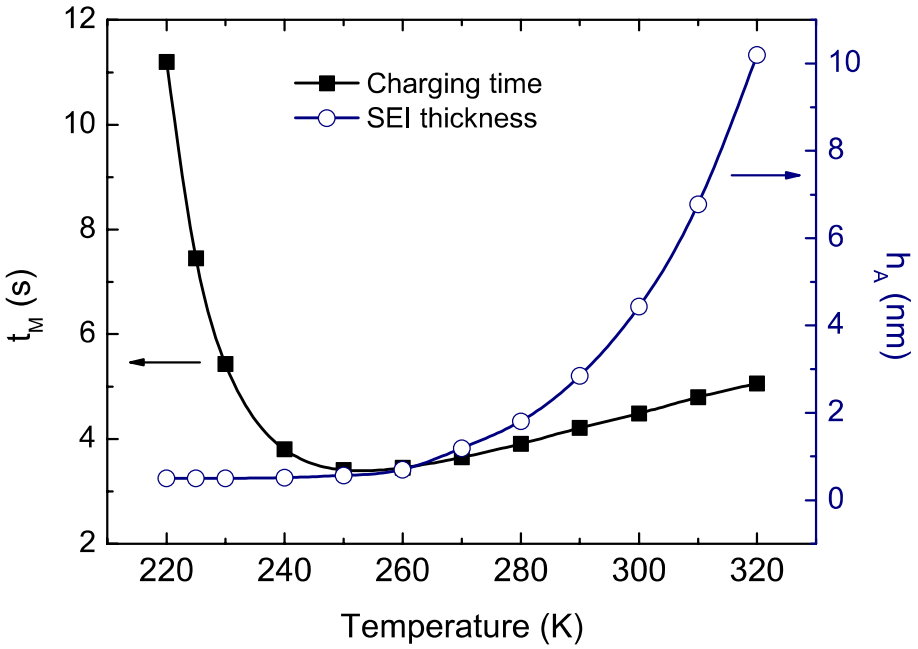

Fig. 6. Temperature effect on the total charging time and SEI thickness during a full charging process.

Fig. 7 displays the SEI growth profile during the first three cycles, but limited to charging processes, because the current KMC model is only developed for the charging operation. At the beginning of each charging process, the electrode is completely discharged, meanwhile the potential in Eq. (8) is applied to the electrode. In this simulation, the activation energies are 46.1 KJ/mol and 69.1 KJ/mol for the Li-ion diffusion and solvent diffusion in SEI, respectively. For the first three charging cycles,

the SEI continues to grow. Nevertheless, the growth rate is reduced with increasing cycle. At the end of these charging cycles, the net SEI growths are 3.14 nm, 1.15 nm, and 0.9 nm. The gradual thickening of the layer accounts for the decreasing trend in SEI growth rate. As the SEI becomes thicker, the absorbed solvent from electrolyte has to transport a longer distance to react with Li-ion with the help of electrons at the electrode-SEI interface, and thus this rate-determining step for SEI formation takes much more time. In contrast, the growing SEI has a negligible impact on Li intercalation into the electrode (no significant change for the total charging time of each cycle, see in Fig. 7(a)), for which the rate-determining step is Li reduction rather than Li-ion diffusion through the SEI layer in Fig. 7(a).

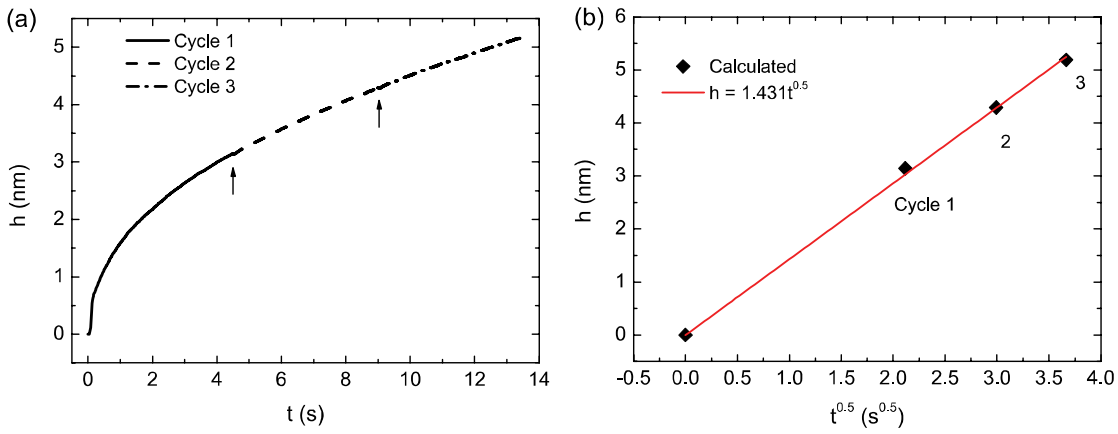

Fig. 7. SEI growth during the first three charging cycles: (a) a function of time and (b) a function of the square root of time. In (b), a linear fitting is computed for the SEI thickness *h* and the square root of time *t*. The activation energies are 46.1 KJ/mol and 69.1 KJ/mol for Li-ion and solvent in SEI, respectively.

Fig. 7(b) shows the SEI thickness as a function of the square root of time over the charging cycles. It is evident that a linear relationship of the two can be well fitted: $h = 1.431t^{0.5}$, and this KMC result is in good agreement with the theoretical models [24]. To further understand the mechanism, we present the theoretical analysis of SEI growth during charging, which is originally from the work by Pinson and Bazant [21]. The rate of SEI thickness h is given as

$$\frac{\mathrm{d}h}{\mathrm{d}t} = K_{SEI}\frac{m}{\rho A} = \frac{N_a}{F}\frac{m}{\rho}J_{SEI}, \text{ where } K_{SEI} = \frac{J_{SEI}A}{F}N_a. \tag{13}$$

Here m is the mass of SEI formed by a single reaction, ρ is the density of SEI, and K_{SEI} is the total number of reactions, directly related to SEI formation, per second on an area of A.

At the electrode-SEI interface, J_{SEI} is exactly proportional to the flux of S-Li$^+$, for instance, the prefactor is $2F$ for the two-electron reduction process. It can be written that

$$J_{SEI} = 2FJ_{S-Li^+} = 2FD\frac{c_{M(S-Li^+)} - c_{S-Li^+}}{h} = 2FD\frac{c_{M(S)} - c_S}{h}, \tag{14}$$

which implies that $c = c_{M(S-Li^+)} = c_{M(S)}$ at the SEI-electrolyte interface and $c = c_{S-Li^+} = c_S$ at the electrode-SEI interface if Li reduction is the rate-determining step, and the contribution from the potential gradient is neglected for the diffusion of neutral solvent. In most cases, D can be considered as the diffusion coefficient of solvent in SEI because of the much faster Li diffusion over solvent diffusion.

By combining Eq. (5), (6), (13), and (14), it can be derived that

$$\left(\frac{h}{D} + \frac{c_{M(S-Li^+)}}{C_{SEI}} \frac{2F}{\sinh\left(-\frac{0.5F}{RT} \eta_{SEI} \right)} \right) \mathrm{d}h = 2N_a \frac{m}{\rho} c_{M(S-Li^+)} \mathrm{d}t, \tag{15}$$

where $\alpha_{SEI} = \beta_{SEI} = 0.5$ is used for Eq. (5). It should be noted that according to Eq. (7) and (8), η_{SEI} is varied with time during a charging cycle. Assuming that φ is a function of η_{SEI} and the capacity fading is negligible, the integral of φ is constant during arbitrary charging cycle *N*

$$\int_{(N-1)t_M}^{Nt_M} \varphi(\eta_{SEI}) \mathrm{d}t = t_M \varphi(\overline{\eta}_{SEI}). \tag{16}$$

Therefore, Eq. (15) is analytically solved to obtain the SEI thickness

$$h = \sqrt{\left(\frac{c_{M(S-Li^+)}}{C_{SEI}} \frac{FD}{\sinh\left(-\frac{0.5F}{RT} \overline{\eta}_{SEI} \right)} \right)^2 + 4N_a D c_{M(S-Li^+)} \frac{m}{\rho} t} - \frac{c_{M(S-Li^+)}}{C_{SEI}} \frac{FD}{\sinh\left(-\frac{0.5F}{RT} \overline{\eta}_{SEI} \right)} \tag{17}$$

It should be noted that *t* can only be the values of Nt_M, where t_M is the total time for a single charging process. As a result, *h* and *t* are discretized by charging cycles. From the above derivation, it is readily apparent that the SEI thickness is not proportional to the square root of time during a single charging cycle. The linear relationship holds in terms of discrete times over cycles in the large time limit, which confirms the KMC results in Fig. 7(b). In addition, Eq. (17) indicates the SEI growth depends little on the charging rate [21].

In reality, there is a multiphase SEI growing on the electrode surface. As shown in Fig. 8, two components of A (purple) and B (white) are considered. Here, Li-ion transport in component B is assumed to be extremely slow. In this regard, the activation

energies of Li-ion diffusion in SEI are 46.1 KJ/mol for A and 65.3 KJ/mol for B, which means that the diffusion rate in A is over 2200 times that in B, and the solvent activation energy is fixed at 67.2 KJ/mol. The effects of the volume ratio of B are depicted in Fig. 8(c). As the volume ratio increases, the total charging time increases, leading to a thicker SEI film for the first charging cycle. It is worth pointing out that the total charging time and SEI growth have non-linear relationships with the volume ratio of B. Fig. 8(a) and (b) illustrate the configurations of SEI film, with the volume ratios of 5% and 33%, and the increasing volume ratio of B could form the network hindering the fast transport pathways in component A.

In Fig. 8(d), it is interesting to observe that Li-ion content varies up-and-down along the depth direction in SEI, and the fluctuation turns to be larger with increasing volume ratio of B. In contrast, for the homogenized SEI, Fig. 4(b) exhibits a predominantly linear Li-ion content trend near the electrode-SEI interface. The non-uniform distribution of component B largely accounts for the fluctuation in Li-ion content. Compared to the fast Li-ion diffusion in component A, Li-ions seems to be trapped after they enter the component B. Therefore, this “trapping effect”, along with the non-uniform distribution of B, induces the results in Fig. 8(d). Moreover, Li-ion diffusion in SEI could become the rate-determining step to govern the overall electrode reactions when the volume ratio of B is large enough.

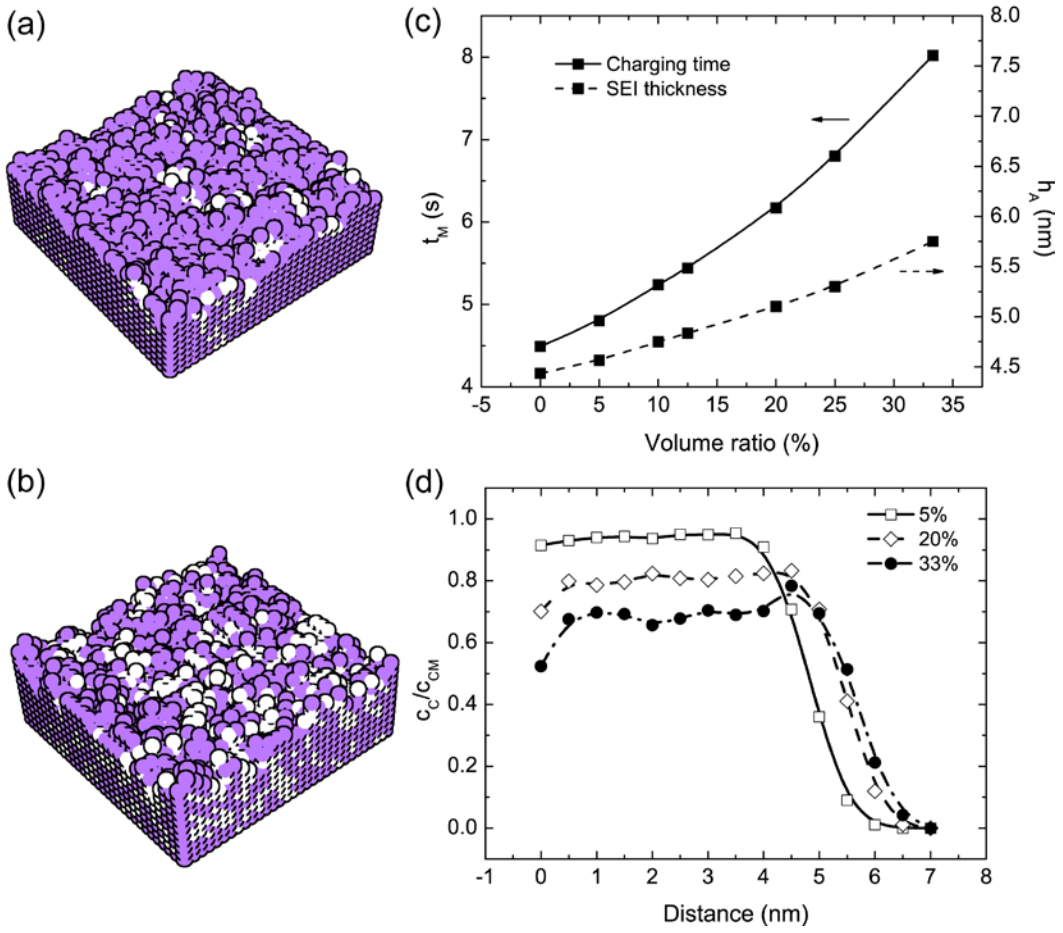

Fig. 8. SEI is composed of two components: purple is A and white is B. The activation energies of Li diffusion are 46.1 KJ/mol and 65.3 KJ/mol in A and B, respectively. SEI morphologies when the volume ratios of component B are 5% in (a) and 33% in (b). (c) The total charging time and SEI thickness with varying volume ratios of B for the first charging process. (d) Li content profiles for various volume ratios of B.

4. Conclusion

In summary, we investigate the negative electrode reactions, composed of mass

transport, Li-ion reduction, and SEI formation, by performing Kinetic Monte Carlo simulations. The results show that the charging time strongly depends on the Li-ion diffusion kinetics in the SEI layer. For instance, increasing the activation energy of Li diffusion reduces the Li-ion concentration at the electrode-SEI interface, thereby increasing the mass-transfer overpotential and SEI thickness. The SEI growth rate directly relies on the operating temperature and the kinetics of solvent diffusion through the SEI film. The KMC simulations demonstrate that the SEI thickness is proportional to the square root of time over charging cycles, which is verified by our theoretical analysis, and the analysis also indicates that the SEI growth depends little on the cycling rate in the limit of long times. In addition, the heterogeneous SEI, consisting of multi-components, could induce Li-ions to be trapped in the components with large activation energies. Based on the KMC model, it confirms the previous studies and reveals some new findings, like the fluctuant Li-ion content in multi-phase SEI film. In the future, the discharging cycle described by KMC models also needs to be included for a comprehensive understanding of SEI growth.

Acknowledgement

The information, data, or work presented herein was funded in part by the Office of Energy Efficiency and Renewable Energy (EERE), U.S. Department of Energy, under Award DE-EE0007766.

References

(1) Larcher, D.; Tarascon, J. M. Towards greener and more sustainable batteries for electrical energy storage. Nat. Chem. **2015**, 7, 19-29.

(2) Lu, L.; Han, X.; Li, J.; Hua, J; Ouyang, M. A review on the key issues for lithium-ion battery management in electric vehicles. J. Power Sources **2013**, 226, 272-288.

(3) Arora, P.; White, R. E.; Doyle, M. Capacity fade mechanisms and side reactions in lithium-ion batteries. J. Electrodchem. Soc. **1998**, 145, 3647-3667.

(4) Aurbach, D.; Moshkovich, M.; Cohen, Y.; Schechter, A. The study of surface film formation on noble-metal electrodes in alkylcarbonates/Li salt solutions, using simultaneous in situ AFM, EQCM, FTIR, and EIS. Langmuir **1999**, 15, 2947-2960.

(5) An, S. J.; Li, J; Daniel, C.; Mohanty, D.; Nagpure, S.; Wood III, D. L. The state of understanding of the lithium-ion-battery graphite solid electrolyte interphase (SEI) and its relationship to formation cycling. Carbon **2016**, 105, 52-76.

(6) Buqa, H.; Würsig, A.; Vetter, J.; Spahr, M. E.; Krumeich, F.; Novák, P. SEI film formation on highly crystalline graphitic materials in lithium-ion batteries. J. Power Sources **2006**, 153, 385-390.

(7) Buqa, H.; Grogger, C.; Alvarez, M. V. S.; Besenhard, J. O.; Winter, M. Surface modification of graphite anodes by combination of high temperature gas treatment and silylation in nonaqueous solution. J. Power Sources **2001**, 97-98, 126-128.

(8) Peled, E.; Golodnitsky, D.; Ardel, G. Advanced model for solid electrolyte interphase electrodes in liquid and polymer electrolytes. J. Electrodchem. Soc. **1997**, 144, L208-L210.

(9) Takenaka, N.; Suzuki, Y.; Sakai, H.; Nagaoka, M. On electrolyte-dependent

formation of solid electrolyte interphase film in lithium-ion batteries: Strong sensitivity to small structural difference of electrolyte molecules. J. Phys. Chem. C **2014**, 118, 10874-10882.

(10) Yan, J.; Zhang, J.; Su, Y.; Zhang, X.; Xia, B. A novel perspective on the formation of the solid electrolyte interphase on the graphite electrode for lithium-ion batteries. Electrochimica Acta **2010**, 55, 1785-1794.

(11) Yoshida, T.; Takahashi, M.; Morikawa, S.; Ihara, C.; Katsukawa, H.; Shiratsuchi, T.; Yamaki, J. Degradation mechanism and life prediction of lithium-ion batteries. J. Electrodchem. Soc. **2006**, 153, A576-A582.

(12) Bridges, C. A.; Sun, X.; Zhao, J.; Paranthaman, M. P.; Dai, S. In situ observation of solid electrolyte interphase formation in ordered mesoporous hard carbon by small-angle neutron scattering. J. Phys. Chem. C **2012**, 116, 7701-7711.

(13) Leung, K.; Soto, F.; Hankins, K.; Balbuena, P. B.; Harrison, K. L. Stability of solid electrolyte interphase components on lithium metal and reactive anode material surfaces. J. Phys. Chem. C **2016**, 120, 6302-6313.

(14) Soto, F. A.; Ma, Y.; Martinez de la Hoz, J. M.; Seminario, J. M.; Balbuena, P. B. Formation and growth mechanisms of solid-electrolyte interphase layers in rechargeable batteries. Chem. Mater. **2015**, 27, 7990-8000.

(15) Tasaki, K.; Harris, S. J. Computational study on the solubility of lithium salts formed on lithium ion battery negative electrode in organic solvents. J. Phys. Chem. C **2010**, 114, 8076-8083.

(16) Ushirogata, K.; Sodeyama, K.; Okuno, Y.; Tateyama, Y. Additive effect on

reductive decomposition and binding of carbonate-based solvent toward solid electrolyte interphase formation in lithium-ion battery. J. Am. Chem. Soc. **2013**, 135, 11967-11974.

(17) Methekar, R. N.; Northrop, P. W. C.; Chen, K.; Braatz, R. D.; Subramanian, V. R. Kinetic Monte Carlo simulation of surface heterogeneity in graphite anodes for lithium-ion batteries: Passive layer formation. J. Electrodchem. Soc. **2011**, 158, A363-A370.

(18) Christensen, J.; Newman, J. A mathematical model for the lithium-ion negative electrode solid electrolyte interphase. J. Electrodchem. Soc. **2004**, 151, A1977-A1988.

(19) Colclasure, A. M.; Smith, K. A.; Kee, R. J. Modeling detailed chemistry and transport for solid-electrolyte-interface (SEI) films in Li-ion batteries. Electrochimica Acta **2011**, 58, 33-43.

(20) Röder, F.; Braatz, R. D.; Krewer, U. Multi-scale simulation of heterogeneous surface film growth mechanisms in lithium-ion batteries. J. Electrodchem. Soc. **2017**, 164, E3335-E3344.

(21) Pinson M. B.; Bazant, M. Z. Theory of SEI formation in rechargeable batteries: Capacity fade, accelerated aging and lifetime prediction. J. Electrochem. Soc. **2013**, 160, A243-A250.

(22) Ploehn, H. J.; Ramadass, P.; White R. E. Solvent diffusion model for aging of lithium-ion battery cells. J. Electrodchem. Soc. **2004**, 151, A456-A462.

(23) Chang, Y.; Jong, J.; Fey, G. T. Kinetic characterization of the electrochemical intercalation of lithium ions into graphite electrodes. J. Electrodchem. Soc. **2000**, 147, 2033-2038.

(24) Swamy, T.; Chiang; Y. Electrochemical charge transfer reaction kinetics at the silicon-liquid electrolyte interface. J. Electrodchem. Soc. **2005**, 162, A7129-A7134.

(25) Bryngelsson, H.; Stjerndahl, M.; Gustafsson, T.; Edström, K. How dynamic is the SEI? J. Power Sources **2007**, 174, 970-975.

(26) Borodin, O.; Zhuang, G. V.; Ross, P. N.; Xu, K. Molecular dynamics simulations and experimental study of lithium ion transport in dilithium ethylene dicarbonate. J. Phys. Chem. C **2013**, 117, 7433-7444.

(27) Shi, S.; Qi, Y.; Li, H.; Hector Jr, L. G. Defect thermodynamics and diffusion mechanisms in Li_2CO_3 and implications for the solid electrolyte interphase in Li-ion batteries. J. Phys. Chem. C **2013**, 117, 8579-8593.

(28) Tokranov, A.; Sheldon, B. W.; Lu, P.; Xiao, X.; Mukhopadhyay, A. The origin of stress in the solid electrolyte interphase on carbon electrodes for Li ion batteries. J. Electrodchem. Soc. **2014**, 161, A58-A65.

Table of Content (TOC) graphic

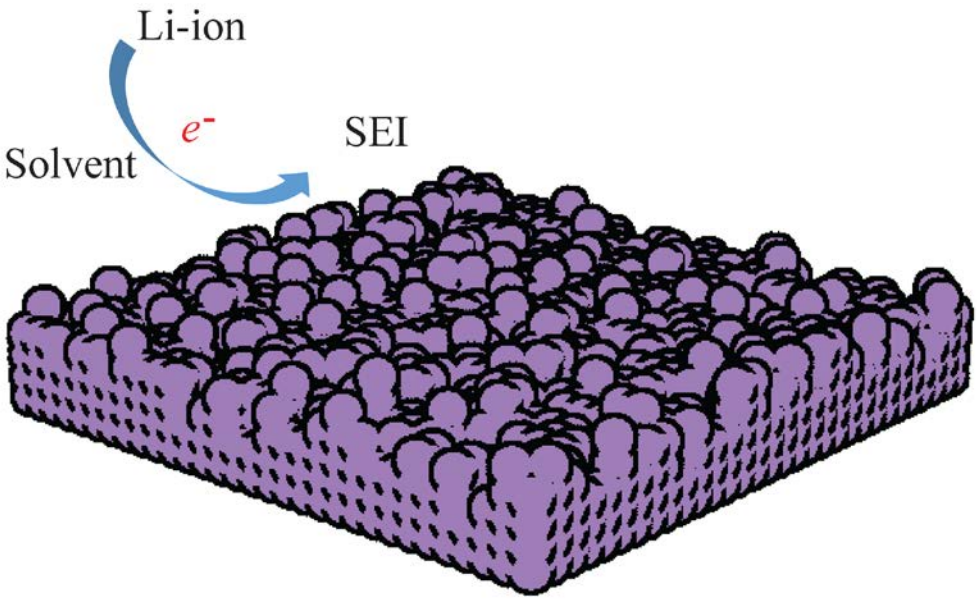
Li-ion
e-
SEI
Solvent